Quantitative analysis of a Hall system in the exhaust of asymmetric magnetic reconnection

Y C Zhang, B Lavraud, L Dai, C Wang, Aurélie Marchaudon, L Avanov, J Burch, M Chandler, J Dorelli, S P Duan, et al.

AGU PUBLICATIONS

JGR

Journal of Geophysical Research: Space Physics

RESEARCH ARTICLE
10.1002/2016JA023620

Key Points:
- Quantification of Hall magnetic field induction by the measured Hall current system using Biot-Savart's law
- Ion pressure gradients support a normal Hall electric field across the exhaust region
- Hall system pattern consistent with kinetic Alfven wave theory also in the exhaust

Correspondence to:
Y. C. Zhang,
zyc@nssc.ac.cn

Citation:
Zhang, Y. C., et al. (2017), Quantitative analysis of a Hall system in the exhaust of asymmetric magnetic reconnection, *J. Geophys. Res. Space Physics*, *122*, 5277–5289, doi:10.1002/2016JA023620.

Received 26 OCT 2016
Accepted 1 MAY 2017
Accepted article online 15 MAY 2017
Published online 20 MAY 2017

Quantitative analysis of a Hall system in the exhaust of asymmetric magnetic reconnection

Y. C. Zhang[1,2,3,4], B. Lavraud[3,4], L. Dai[1], C. Wang[1], A. Marchaudon[3,4], L. Avanov[5,6], J. Burch[7], M. Chandler[8], J. Dorelli[5], S. P. Duan[1], R. E. Ergun[9], D. J. Gershman[5,6], B. Giles[5], Y. V. Khotyaintsev[10], P. A. Lindqvist[11], W. Paterson[5], C. T. Russell[12], C. Schiff[5], B. B. Tang[1], and R. Torbert[13]

[1]State Key Laboratory of Space Weather, National Space Science Center, Chinese Academy of Sciences, Beijing, China, [2]Key Laboratory of Earth and Planetary Physics, Institute of Geology and Geophysics, Chinese Academy of Sciences, Beijing, China, [3]Institut de Recherche and Astrophysique et Planétologie, Université de Toulouse (UPS), Toulouse, France, [4]Centre National de la Recherche Scientifique, Toulouse, France, [5]NASA Goddard Space Flight Center, Greenbelt, Maryland, USA, [6]Department of Astronomy, University of Maryland, College Park, Maryland, USA, [7]Southwest Research Institute, San Antonio, Texas, USA, [8]NASA Marshall Space Flight Center, Huntsville, Alabama, USA, [9]Laboratory of Atmospheric and Space Physics, University of Colorado Boulder, Boulder, Colorado, USA, [10]Swedish Institute of Space Physics, Uppsala, Sweden, [11]Royal Institute of Technology, Stockholm, Sweden, [12]University of California, Los Angeles, Los Angeles, USA, [13]Physics Department, University of New Hampshire, Durham, New Hampshire, USA

Abstract Taking advantage of high-resolution measurements from the MMS mission, we find evidence for a complete Hall system in the exhaust of asymmetric magnetic reconnection 40 D_i downstream of the X line. The investigation of the fine structure of the Hall system reveals that it displays features in the exhaust similar to those reported previously in the ion diffusion region by simulations and observations. This finding confirms the importance of particle-scale processes in the reconnection exhaust as well. On the magnetospheric side of the exhaust, electrons are strongly accelerated by parallel electric fields. This process significantly contributes to feed the Hall current system, resulting in a nonnegligible Hall magnetic field signature on this side despite an otherwise lower density. Calculation of the induced out-of-plane magnetic field by in-plane currents (based on Biot-Savart law) provides direct quantitative evidence for the process of Hall magnetic field generation by the Hall current system. A strong normal Hall electric field is present only on the magnetospheric side of the exhaust region, consistent with previous works. Multipoint data analysis shows that the ion pressure gradient in the ion momentum equation produces this Hall electric field. This global pattern of the Hall system can be explained by kinetic Alfvén wave theory.

1. Introduction

Collisionless magnetic reconnection is characterized by a Hall system, which is typically confined to the ion diffusion region [*Sonnerup*, 1979]. The existence of this Hall system has major implications with regard to the reconnection process and associated particle dynamics in the diffusion region [*Mandt et al.*, 1994; *Shay et al.*, 2001; *Wang et al.*, 2001; *Xiao et al.*, 2007; *Deng and Matsumoto*, 2001]. The Hall magnetic fields are induced by Hall currents as a result of the decoupling of ions and electrons.

Under symmetric conditions, Hall magnetic fields display a quadrupole structure out of the magnetic reconnection plane, while associated electric fields in the reconnection plane display a bipolar structure directed toward the midplane [*Birn et al.*, 2001; *Mozer et al.*, 2002; *Borg et al.*, 2005; *Wygant et al.*, 2005; *Sonnerup et al.*, 2016]. In nature, the conditions for reconnection are often highly asymmetric, however, such as at the dayside magnetopause [*Phan and Paschmann*, 1996]. The asymmetric conditions substantially alter the basic properties of reconnection [*Øieroset et al.*, 2004; *Cassak and Shay*, 2007, 2008] and the structure of the Hall system [*Mozer et al.*, 2008a; *Pritchett*, 2008]. In simulations, the Hall magnetic field is only observed on the high-density side of the current sheet (magnetosheath side at the dayside magnetopause) [*Pritchett*, 2008; *Malakit et al.*, 2010]. An intuitive explanation for the asymmetry of Hall magnetic fields is that high density on the magnetosheath side provides abundant carriers for Hall currents [*Eastwood et al.*, 2013]. The simulation of *Prichett et al.* [2008] also found that an electric field directed toward the midplane was only present on the magnetospheric side. This feature has been verified by observations from reconnection observations at the dayside magnetopause [*Mozer et al.*, 2008a, 2008b]. Although this electric field (usually called

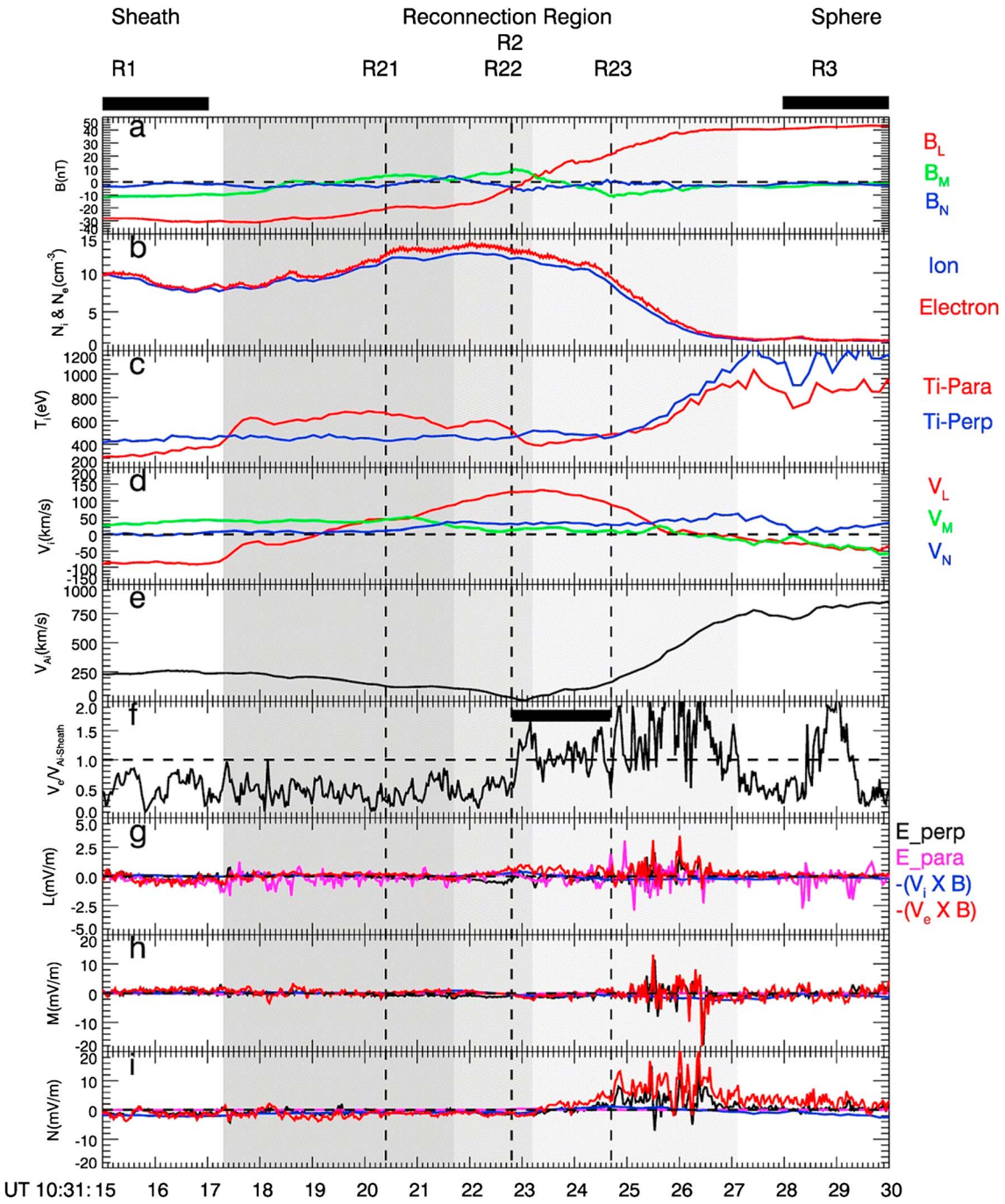

Figure 1. MMS 2 plasma and field observations of the reconnection event on 13 December 2015 in LMN coordinates. In GSE coordinates, L = (0.31, −0.22, 0.93), M = (0.44, −0.83, −0.34), and N = (0.84, 0.51, −0.16). (a) The three components of the magnetic field, (b) ion and electron densities, (c) the ion parallel and perpendicular temperatures, (d) the three components of ion velocity, (e) the ion Alfvén speed, (f) the electron Alfvénic Mach number, and (g–i) the L, M, and N components of the perpendicular electric field $\boldsymbol{E}_{\perp}$, parallel electric field $\boldsymbol{E}_{\parallel}$,$-(\boldsymbol{V_e} \times \boldsymbol{B})$, and $-(\boldsymbol{V_i} \times \boldsymbol{B})$, respectively. The exhaust region R2 is shaded grey, with three subregions (R21–R23) as discussed in the text. Regions R1 and R3 are intervals representative of the magnetosheath and magnetosphere, respectively.

the Hall electric field) was found to be balanced by the Hall term in the generalized Ohm's law [*Khotyaintsev, et al.*, 2006; *Mozer et al.*, 2008a], the mechanism behind the generation of this electric field has been the subject of many recent studies. Theory first explained this electric field for the nonreconnecting magnetopause in terms of finite Larmor radius effect [*Cowley*, 1995]. Recent observational results also support this point [*Aunai et al.*, 2011; *Dai et al.*, 2015; *Torbert et al.*, 2016; *Wang et al.*, 2016]. Although most

investigations of the Hall physics has been performed in the ion diffusion region, it was found that the Hall effect may also persist beyond the diffusion region in the magnetotail [*Fujimoto et al*., 1997; *Nagai et al*., 2001; *Øieroset et al*., 2004; *Manapat et al*., 2006] and solar wind [*Mistry et al*., 2017]. Recently, the decoupling of ions and electrons was also observed in the reconnection exhaust at the dayside magnetopause [*Phan et al*., 2016a]. These studies thus suggest that the Hall physics also plays a role in the dynamics of the reconnection exhaust.

The four NASA MMS [*Burch et al*., 2015] spacecraft were launched together on 12 March 2015 on an Atlas V launch vehicle into a highly elliptical 28° inclination orbit with perigee at 1.2 Earth radii (R_E) and apogee at 12 R_E. In this study, we investigate the Hall system (magnetic fields, electric fields, and currents system) in an asymmetric reconnection event observed by the MMS satellites at the dayside magnetopause. We primarily focus on ion and electron measurements from the Fast Plasma Instruments [*Pollock et al*., 2016], magnetic field measurements from the fluxgate magnetometers [*Russell et al*., 2015] and electric field measurements from the Axial Double Probes and Spin-plane Double Probes [*Torbert et al*., 2014]. These unprecedented high-resolution measurements make it possible to analyze the fine structure of the Hall system. The analysis demonstrates new features of the Hall system in the exhaust of magnetic reconnection. These may be explained by means of kinetic Alfvén wave (KAW) theory, similar to the Hall physics in the ion diffusion region. Also, owing to the lack of appropriate observations before MMS, there have, so far, been no direct and quantitative study demonstrating that measured Hall magnetic fields are induced by measured Hall currents. Here we use a method based on Biot-Savart's law to quantitatively demonstrate this relationship. Observations of reconnection and its background conditions from MMS observation are presented in section 2. We then provide a detailed multispacecraft analysis of the Hall system and discuss its implications in section 3. Discussions and summary are provided in section 4.

2. Reconnection Observations: Overview

Figure 1 displays the observations from the MMS 2 satellite during 10:31:15 UT–10:31:30 UT on 13 December 2015 in the local LMN coordinates [*Sonnerup and Scheible*, 1998] of the magnetopause. The separation between the four spacecraft was ~10 km, so observations from all four spacecraft show similar overall behaviors. Only the data from MMS 2 are used, unless otherwise mentioned such as for the analyses based on multiple-point observations. In Figure 1, depending on the different features of the measured plasma, the observations are separated into three main distinct regions using white and grey colors. Region R1, in white with the first horizon black bar, marks the magnetosheath region, which has a southward magnetic field (Figure 1a), high plasma density (Figure 1b), and ion temperature anisotropy with $Ti_\perp > Ti_\parallel$ (Figure 1c). Region R3, in white with the second horizon black bar, marks the magnetosphere, which has a northward magnetic field and low plasma density. The plasma flows in R1 and R3 are very slow with the speed of about tens of km/s along the $-L$ direction (Figure 1d). Region R2, in grey, marks the reconnection region, in which magnetic fields display more fluctuation than in R1 and R3 and reconnection jets are present with a peak value at ~142 km/s (Figure 1d). The reconnection region R2 has a duration of ~10 s. The reconnection jet is aligned with the $+L$ (northward) direction. Therefore, the MMS satellite crosses the northern branch of the reconnection region from the magnetosheath to the magnetosphere. This is shown with the red spacecraft trajectory in Figure 2. While the magnetosheath is typically flowing at $V_L \sim -80$ km/s, the reconnection jet reaches near 222 km/s. This is about 90% of the Alfvén speed (~250 km/s based on the magnitude of B_L component) (Figure 1e) in the magnetosheath.

Comparison of the measured perpendicular electric field $\boldsymbol{E}_\perp$, $\boldsymbol{E}_\parallel$,$-(\boldsymbol{V_e} \times \boldsymbol{B})$, and $-(\boldsymbol{V_i} \times \boldsymbol{B})$ in Figures 1g–1i shows a good correlation between $\boldsymbol{E}_\perp$ and $-(\boldsymbol{V_e} \times \boldsymbol{B})$, but a poor correlation between $\boldsymbol{E}_\perp$ and $-(\boldsymbol{V_i} \times \boldsymbol{B})$. The electrons are frozen-in, but ions are not. Recently, this has been observed with MMS in the exhaust region [*Phan et al*., 2016a] and in small flux ropes [*Eastwood et al*., 2016]. So one should not identify this as the ion diffusion region around the X line, but only as a region where the ions are not frozen-in inside the exhaust.

We apply four spacecraft timing analysis [*Russell et al*., 1983; *Schwartz*, 1998] to the crossing of this reconnection region. Based on the B_L reversal, the normal direction of the magnetopause is determined along [0.85, 0.50, −0.17] in GSE and the normal speed is +65 km/s. Considering a crossing time of about 10 s, the reconnection region is estimated to have a thickness of 650 km, or 8.0 times the ion inertial length D_i. If the reconnection

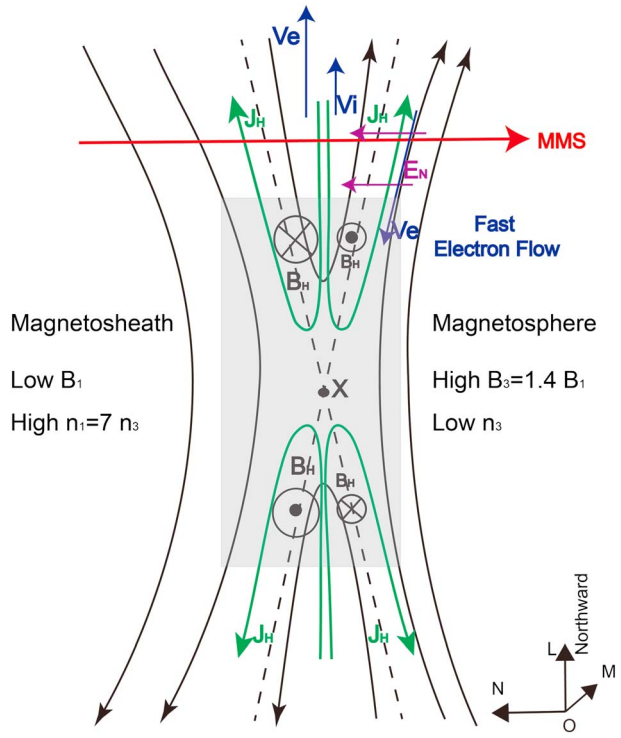

Figure 2. Sketch depicting asymmetric reconnection and its associated Hall system, with the local coordinates [*L*, *M*, *N*] superimposed on the right. The grey shaded area indicates the ion diffusion region. The magnetosheath is to the left and the magnetosphere to the right. Solid black curves indicate magnetic field lines, and solid green curves indicate the Hall current system. Dashed black lines indicate the separatrices which intersect at the X line. The purple lines with arrows indicate the electric field in the normal (*N*) direction. The blue lines with arrows indicate the electron and ion flows, roughly in the *L* direction, respectively. The red line with an arrow indicates the MMS trajectory across the exhaust, outside the ion diffusion region.

region aspect ratio (of the width to the thickness of the reconnection region) is assumed to be 10 [*Zenitani et al.*, 2011], the MMS distance from the X line is 40 D_i, which is beyond typical diffusion region extents.

Simulation results show that in the midplane of the diffusion region the electron velocity can reach electron Alfvén speed [*Karimabadi et al.*, 2007] and is super-Alfvénic [*Fujimoto and Takamoto*, 2016] based on conditions upstream of the reconnection region, while outside the diffusion region electrons slow down to ion Alfvén speed [*Karimabadi et al.*, 2007; *Fujimoto and Takamoto*, 2016]. This signature was verified in previous observations [*Nagai et al.*, 2013]. Figure 1f displays the electron Alfvénic Mach number ($V_e/V_{Ai\text{-}sheath}$, $V_{Ai\text{-}sheath}$ is the ion Alfvén speed in the upsteam magnetosheath). In the midplane indicated by the horizontal black bar in Figure 1f, the electron Alfvénic Mach number only reaches the values of about 1, showing that electrons are Alfvénic.

Therefore, the Alfvénic nature of the electron flows in the midplane, the agreement between the observed ion jet and the Alfvén speed, and the estimation of the distance to the X line all indicate that Region 2 (grey) in Figure 1 is the exhaust of this reconnection event [*Paschmann et al.*, 1979]. To evaluate the background conditions on either side of this reconnection exhaust, average parameters from the regions marked by horizontal black bars at the top of Figure 1 are considered representative of the magnetosheath and magnetospheric plasmas, respectively. Only the tangential components [*L*, *M*] are taken into account for the evaluation of the background plasma conditions because they are the components involved in the reconnection process [e.g., *Cassak and Shay*, 2007]. The plasma conditions for this reconnection event can be summarized as follows.

On the magnetosheath side,

$$B_1 = [B_{1L}, B_{1M}] = [-29.98\pm1.12, -0.11\pm0.72]\ \text{nT}, n_1 = 9.33\pm1.32\ \text{cm}^{-3};$$

and on the magnetospheric side,

$$B_3 = [B_{3L}, B_{3M}] = [41.94\pm0.71, -1.52\pm0.31]\ \text{nT}, n_3 = 1.25\pm0.10\ \text{cm}^{-3}.$$

The errors given are the standard deviations from the average in each background condition interval. The asymmetry is rather weak in magnetic field magnitude with $|B_3|/|B_1| = 1.38 \pm 0.13$ but high in plasma density with $n_1/n_3 = 7.46 \pm 1.24$. The magnetic shear angle ($\theta°$) is 160.1° ± 4.7°, as calculated by $\theta° = \text{acos}(\boldsymbol{B}_1 \cdot \boldsymbol{B}_3)$. A shear angle of 160° corresponds to a guide field of approximately 18% of the reconnecting fields, i.e., the guide field in this case is ~−6 nT or so. Simulations and laboratory experiments show that such a guide field produces noticeable changes in the reconnection features compared to cases without guide field [*Karimabadi et al.*, 2005; *Swisdak et al.*, 2005; *Tharp et al.*, 2012]. Observations and modeling have shown, in particular, that the presence of a guide field significantly distorts the topology of the Hall system in the diffusion region [*Mozer et al.*, 2008a; *Pritchett*, 2008; *Eastwood et al.*, 2010].

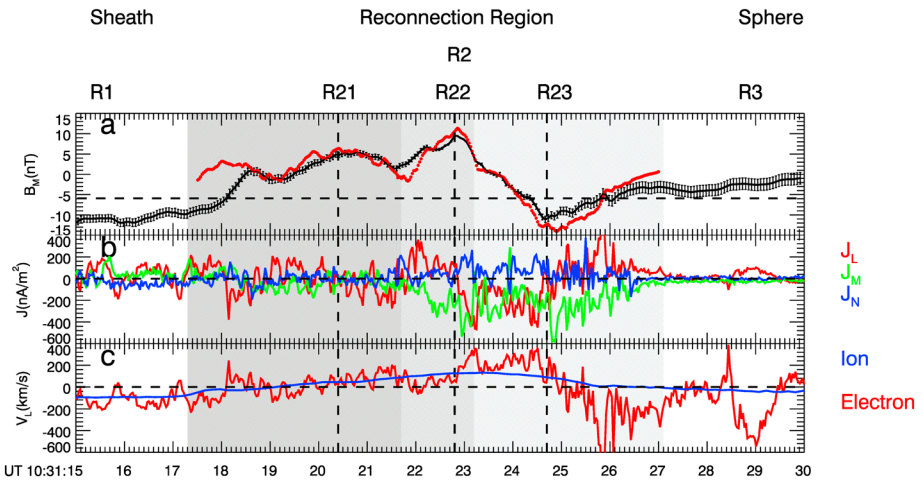

Figure 3. MMS observations of the Hall current and magnetic field system. (a) B_M averaged over the results from 78 MVAB analyses with the estimated B_M from Biot-Savart's law superimposed, (b) the three components of the current density from particle measurements, and (c) ion and electron velocity component in L direction. The exhaust region is shaded grey.

3. Analysis of the Hall System

3.1. Asymmetric Hall Magnetic Fields

In the exhaust region (R2), at 10:31:23.2 UT, B_L changes from negative to positive, and B_M almost simultaneously changes from positive to negative (Figure 1a). B_N, however, maintains a negative direction at this time, which is consistent with the scenario of open magnetic fields on the northern side of the X line (Figure 2). A notable feature in the exhaust region is the variation of B_M. The B_M polarity is consistent with the Hall magnetic fields expected in the diffusion region northward of the X line (Figure 2) for the given crossing. A Hall magnetic field signature is clearly present on both sides of the exhaust region in this crossing. It should be noted that a dip in B_M is present at 10:21:07 UT, on the magnetosheath side of the exhaust (Figures 1a and 3a). On the magnetosheath side, the Hall magnetic field thus shows two main positive peaks. On the magnetosphere side, the Hall magnetic field B_M has only one negative peak. The three peaks in B_M are marked by three separate dashed lines at 10:31:20.4 UT, 10:31:22.8 UT, and 10:31:24.7 UT. To facilitate the following analysis the exhaust region is divided into three subregions, labeled R21, R22, and R23, each with different intensities of grey, and every one of which covers one of the unipolar B_M variations (associated with the three B_M peaks). R22 and R23 are adjacent to the B_L turning from the magnetosheath to the magnetosphere side. Region R21 is sunward of R22. To test whether the B_M peak in R21 is simply a partial crossing back into the B_M peak in R22 due to a back and forth motion of the Hall region, four spacecraft timing analysis [*Russell et al*., 1983; *Schwartz*, 1998] is applied to the signatures of the three B_M peaks separately. The results show that first B_M peak is moving with the velocity of [66.05, 6.33, −12.74] km/s in GSE. The velocity for other two B_M peaks are consistently found as [65.13, 11.56, −12.39] km/s and [66.67, 12.16, −10.78] km/s in GSE, respectively. These magnetic structures always maintain an outward motion away from the Earth. This indicates that the B_M peaks in R21 and R22 are separate spatial magnetic structures.

As mentioned before, the guide field is ~−6 nT in this case. We set −6 nT as a baseline to evaluate the magnitude of Hall magnetic fields [*Øieroset et al*., 2001, 2004]. As shown in Figure 3a, relative to the baseline on the magnetosheath side the positive Hall fields have a peak value of +15.2 nT (the second vertical dash line), while on the magnetosphere side the negative Hall field has a peak value of −5.1 nT (third vertical dashed line). Such asymmetric Hall magnetic fields have been observed in the diffusion region of asymmetric reconnection in past works (observations and simulations). A prominent Hall magnetic field signature is only expected on the magnetosheath side of the diffusion region [*Mozer et al*., 2008a; *Malakit et al*., 2010; *Phan et al*., 2016b]. How such asymmetric Hall magnetic fields are generated in the exhaust will be explained in next section.

Here it should be noted that the determination of the LMN coordinate system is important for the estimation of B_M. Because we aim to investigate the magnetic field structure in the entire exhaust region, the time interval used for minimum variance analysis of B (MVAB) analysis must comprise the entire exhaust region

(grey color between 10:31:17 UT and 10:31:27 UT in Figure 1). We performed 78 MVAB analyses by shifting the start time between 10:31:12 UT and 10:31:17 UT and the end time between 10:31:28 UT and 10:31:40 UT. The black curve in Figure 3a shows the B_M time series averaged over the 78 B_M series resulting from the 78 different LMN coordinates. The error bars indicate the standard deviation from the average over the 78 analyses. The ratio of the Hall magnetic field peak on the magnetosheath side to that on the magnetosphere side is 3.0 (relative to guide field). The maximum ratio is 3.7 and the minimum ratio is 2.5. The Hall magnetic field is thus much larger on the magnetosheath side, as expected. The choice of the interval for minimum variance analysis changes this ratio by ~23% at most, so this choice does not affect the asymmetric nature of the Hall magnetic field (B_M) component. The time interval 10:31:15 UT–20:31:30 UT is selected for the MVAB analysis and LMN coordinates used in the remainder of this paper (with eigenvalue ratios of $\lambda_1/\lambda_2 = 28.5$ and $\lambda_2/\lambda_3 = 10.2$) [*Sonnerup and Scheible*, 1998].

3.2. Hall Current System

The definition of Hall magnetic fields is that they are induced by a Hall current that results from the decoupling of ions and electrons in the ion diffusion region (although as said previously they have been observed to extend outside the ion diffusion region). Only Hall currents transverse to the magnetic field contribute to the Hall term ($J \times B/nq$) in the generalized Ohm's law. However, as shown in the following analysis, the observed reconnection-induced currents have strong field-aligned components as well, so we refer to the ensemble of these currents as the Hall current system instead of just "Hall currents" [*Sonnerup*, 1979; *Alexeev et al*., 2005]. In this section, we investigate the currents adjacent to the observed Hall magnetic fields and the particle decoupling process in relation to the currents. High-resolution MMS data make it possible to calculate the current density directly from the definition of $\boldsymbol{J} = q(n_i\boldsymbol{V_i}\text{-}n_e\boldsymbol{V_e})$, using single-point particle measurements [e.g., *Burch et al*., 2016; *Lavraud et al*., 2016]. The resulting currents are shown in Figure 3b. The in-plane J_L is the major component responsible for inducing the out-of-plane B_M magnetic field. In region R22, the J_L direction is first positive and changes to negative at the peak of B_M. J_L maintains a negative direction in the midplane region across R22 and R23. In region R23, the J_L direction changes back to positive at the negative peak of B_M (third dashed line). The direction of J_L thus indicates that the current is flowing around the Hall magnetic field. J_L experiences a nearly symmetric V-type variation with a peak value of 400 nA/m^2 in the positive direction and -400 nA/m^2 in the negative direction. So it is reasonable to say that J_L is the main component that contributes to the Hall current system inducing the Hall magnetic field. The positive J_L corresponds to Hall currents flowing away from the X line on the magnetosheath and magnetosphere side, while the negative J_L corresponds to Hall currents flowing toward the X line along the magnetopause in the midplane region. These currents are illustrated in Figure 2.

To quantitatively verify this hypothesis, the out-of-plane magnetic fields B_M induced by in-plane currents are estimated using a method that directly employs the Biot-Savart law:

$$\boldsymbol{B}(\boldsymbol{r}) = \frac{\mu_0}{4\pi}\int_V \frac{\boldsymbol{J}(V)\times\boldsymbol{r}}{r^3}\mathrm{d}V, \tag{1}$$

where $\boldsymbol{B}(\boldsymbol{r})$ is the magnetic field at position $\boldsymbol{r}$ relative to the source current $\boldsymbol{J}$ in the spacial volume $\boldsymbol{V}$ ($\boldsymbol{V}$ is the volume containing the current $\boldsymbol{J}$). For the calculation of B_M at position (l_0,m_0,n_0) equation (1) can be written as follows:

$$B_M(l_0, m_0, n_0) = \frac{\mu_0}{4\pi}\int_l\int_m\int_n \frac{(J_N(l-l_0) - J_L(n-n_0))}{r^3}\mathrm{d}l\mathrm{d}m\mathrm{d}n, \tag{2}$$

where l, m, and n denote the position in the LMN coordinates and $r = \sqrt{(l-l_0)^2 + (m-m_0)^2 + (n-n_0)^2}$. In our estimation, only the term J_L of the current density is considered, because the transverse crossing of MMS, i.e., normal to the magnetopause (Figure 3b), only permits to sample the J_L distribution along N while not the J_N distribution along L. The contribution of the term with J_N should be small, in any case, as the intensity of J_N is much lower than that of J_L (Figure 3b). J_L is assumed to be steady and evenly distributed in the L and M directions. As we do not know the dimensions of the J_L distribution in the L and M directions, the integration domain in equation (2) is assumed to be infinity in both directions. In Biot-Savart law (equation (1)), the magnetic field magnitude cubic decrease with distance to the current source means that remote currents have an insignificant contribution to the magnetic field. The dimension in the N direction is calculated using $n = tV_n$, where t is the spacecraft crossing duration through

the Hall current region and V_n is the normal speed of the Hall structure relative to the spacecraft as estimated through four spacecraft timing analysis.

The estimated out-of-plane magnetic field is displayed with a red dotted curve in Figure 3a. It fits very well the measured B_M throughout the exhaust except near the edge with the magnetosheath. This calculation of the Hall magnetic field based on Biot-Savart law provides direct quantitative evidence for the process of Hall magnetic field generation by the Hall current system. The analysis also shows that J_L is first positive and then changes to negative at the peak of B_M in both regions R21 and R22 (shaded areas in Figure 3). All four MMS spacecraft observed this feature (not shown here). Since we have shown that these features are spatial rather than temporal in nature, these results support the idea that the Hall current system on the magnetosheath side comprises two Hall-type current systems (where B_M is induced by the surrounding currents that change direction from north to south).

The Hall currents can also be studied directly from the particles behavior. According to the definition of current density, $\boldsymbol{J} = q(n_i\boldsymbol{V_i} - n_e\boldsymbol{V_e})$, particle density and velocity are responsible for the final $\boldsymbol{J}$. Since $n_i \approx n_e$ (Figure 1b), the current density is determined by the plasma density n and the ion-electron velocity difference $\boldsymbol{V_i} - \boldsymbol{V_e}$. Throughout the Hall regions R22 and R23, the decoupling of ions and electrons is clearly observed (Figures 1g–1i). Figure 3c displays the L components of the ion and electron velocities. In the midplane, across the magnetopause between the second and third dashed vertical lines in Figure 3, the positive electron velocity is larger than the positive ion velocity, so that it produces strong currents in the $-L$ direction. In region R22 before the second vertical dashed line, and in region R23 after the third vertical dashed line, the ion velocity remains positive but the electrons flow along $-L$, producing $+L$ currents. The $-L$ currents at the midplane and $+L$ currents on the magnetosheath and magnetospheric sides form together the complete set of Hall currents. The $+L$ current and $-$L currents have a similar peak value of approximately 400 nA/m^2.

Figure 3c shows that the velocity difference in the L direction is small on the magnetosheath side of the exhaust. As explained in past works [*Eastwood et al*., 2013] the strong Hall currents are supported by the high plasma density there. However, the situation is different on the magnetospheric side (region after the third vertical dashed line). The plasma density decreases to about 1/7 of the plasma density on the magnetosheath side. However, the inward ($-L$ direction) electron velocity reaches up to 560 km/s. It is thus the high electron velocity that supports the Hall currents on the magnetospheric side. The L component of the parallel electric fields have values up to 2 mV/m, consistent with the acceleration of electrons to high velocities as observed on the magnetospheric side (Figure 1g). The resulting electron jet contributes to the strong Hall currents by compensating the lack of plasma density. Such parallel electric fields may have a large scale, as reported by *Egedal et al*. [2005, 2008]. Recently, *Fujimoto* [2014] found in simulations that in addition to coherent parallel electric fields, bipolar solitary waves can be very efficient in the separatrix region to accelerate electrons and trigger wave activity. The fluctuating electric field in Figures 1g–1i shows that wave activity is associated with the observed fast electrons. For this asymmetric reconnection case, we quantified the role of the Hall current system that produces the Hall magnetic fields by the decoupling of ions and electrons. We showed that particularly strong parallel electric fields are observed on the magnetospheric side. These sustain the strong electron velocities in L direction that are required to feed the Hall current system and in turn generate the Hall magnetic fields on this tenuous side of the asymmetric magnetopause.

3.3. Asymmetric Hall Electric Fields

Another asymmetric feature of the Hall system observed in the exhaust of this asymmetric case is a strong component of the (Hall) electric field normal to the magnetopause, as shown by the measured E_N in Figure 1i. E_N has an average value on the order of -1.4 mV/m on the magnetosheath side and a peak value of ~7.1 mV/m on the magnetospheric side. E_N points toward the midplane from the magnetosheath to magnetosphere and the change in direction occurs near the B_L zero crossing. The observations thus show a strong E_N on the magnetosphere side far from the ion diffusion region, downstream in the exhaust (R23). The presence of such a normal electric field at the magnetopause has been put forward from theoretical considerations [*Cowley*, 1995] and has been measured in situ previously in the diffusion region[*Vaivads et al*., 2004; *Andre et al*., 2004; *Mozer et al*., 2008a; *Pritchett*, 2008; *Malakit et al*., 2010; *Phan et al*., 2016b].

Several mechanisms have been proposed to explain its existence in the ion diffusion region. By comparing $(\boldsymbol{E} + \boldsymbol{V_i} \times \boldsymbol{B})_{\boldsymbol{N}}$ and $(\boldsymbol{J} \times \boldsymbol{B})_N/nq$, the normal electric field was found to be balanced by the Hall MHD term in

the general Ohm's law [*Vaivads et al*., 2004; *Mozer et al*. 2008a], thereby also proving that Hall physics dominates in the diffusion region. However, simulations and theoretical works have shown that the gradient of the plasma pressure tensor may be the source of plasma defreezing from the magnetic and electric fields [*Cai et al*., 1994; *Cai and Lee*, 1997; *Hesse et al*., 2011]. Recently, the contribution of the plasma pressure gradient has been tested with observations in the ion diffusion region [*Aunai et al*., 2011; *Dai et al*., 2015] and electron diffusion region [*Torbert et al*., 2016]. *Burch et al*. [2016] also attribute the normal electric field in the diffusion region to ion pressure gradients. The ion dynamics related to the Hall electric fields in the ion diffusion region has also recently been discussed by *Wang et al*. [2016]. MMS 3-D measurements of electric fields now make it possible to investigate the physical generation mechanism of the normal electric fields associated with Hall magnetic fields. We discuss the mechanism of Hall electric fields in the exhaust of the present reconnection in the following.

Figures 4a and 4b, respectively, display the time series of $\boldsymbol{E}'=\boldsymbol{E}+\boldsymbol{V_i}\times\boldsymbol{B}$ and the Hall term $(\boldsymbol{J}\times\boldsymbol{B})/nq$, both averaged over the four spacecraft measurements. We focus on the normal components in blue in Figure 4. Although the magnitude of $(\boldsymbol{J}\times\boldsymbol{B})_N/nq$ is somewhat larger than $\boldsymbol{E}'_{\boldsymbol{N}}$, their variations are very well correlated. So the Hall term is able to balance $\boldsymbol{E}'_{\boldsymbol{N}}$, as reported in previous works [*Vaivads et al*., 2004; *Mozer et al*. 2008a]. Yet one cannot say that the normal electric field simply results here from the Hall term. The reason is as follows. As shown in Figures 1g–1i, electrons are nearly frozen-in throughout the exhaust region. If we add $\boldsymbol{V_i}\times\boldsymbol{B}$ to both sides of the electron frozen-in equation $\boldsymbol{E}=-\boldsymbol{V_e}\times\boldsymbol{B}$, the relation $\boldsymbol{E}+\boldsymbol{V_i}\times\boldsymbol{B}=(1/nq)\boldsymbol{J}\times\boldsymbol{B}$ is naturally obtained. In other words, $\boldsymbol{E}+\boldsymbol{V_i}\times\boldsymbol{B}=(1/nq)\boldsymbol{J}\times\boldsymbol{B}$ is necessarily established as long as the electron frozen-in condition is satisfied, and we cannot infer the physical relation between $\boldsymbol{E}+\boldsymbol{V_i}\times\boldsymbol{B}$ and $(\boldsymbol{J}\times\boldsymbol{B})/nq$ from this equation. The appropriate equation to obtain the underlying physics of $\boldsymbol{E}+\boldsymbol{V_i}\times\boldsymbol{B}$ is the ion momentum equation:

$$\boldsymbol{E}+\boldsymbol{V_i}\times\boldsymbol{B}=(1/n_iq_i)\nabla\cdot\boldsymbol{P_i}+(m_i/q_i)\mathrm{d}\boldsymbol{V_i}/\mathrm{d}t+(m_i/q_i)\nu_{\boldsymbol{ie}}(\boldsymbol{V_i}-\boldsymbol{V_e}), \tag{3}$$

where P_i is ion pressure tensor and $\nu_{\boldsymbol{ie}}$ is the ion-electron collision frequency. Figures 4c and 4d display the calculation of the ion pressure gradient term $(1/n_iq_i)\nabla\cdot\boldsymbol{P_i}$ and the ion inertial term $(m_i/q_i)\mathrm{d}\boldsymbol{V_i}/\mathrm{d}t$ using MMS data. The calculation method is the same as in *Torbert et al*. [2016]. Comparing with $\boldsymbol{E}'_{\boldsymbol{N}}$ in Figure 4a, it is clear that $(1/n_iq_i)(\nabla\cdot\boldsymbol{P_i})_{\boldsymbol{N}}$ is dominant and $(m_i/q_i)(\mathrm{d}\boldsymbol{V}_i/\mathrm{d}t)_N$ is a minor contributor to $\boldsymbol{E}+\boldsymbol{V_i}\times\boldsymbol{B}$. So the Hall electric field in the exhaust region is mainly supported by the ion pressure gradient. The collision term cannot be directly quantified. Subtraction of the pressure gradient and inertial terms on both sides of the ion momentum equation can give an estimation of the collision term. The results are shown in Figure 4e. It should be noted that collision effects cannot be deemed dominant, so that the large values of the collision term observed at times during this interval may rather be attributed to observational uncertainties (the largest values appear at times of largest gradients and lowest density, as expected for such subtle measurements). The contribution of this deduced collision term to the electric field is thus not discussed further here.

4. Discussions and Summary

Most past works have focused on the asymmetric nature of the Hall system in the diffusion region of asymmetric reconnection. In the present study, a magnetic reconnection event is studied for highly asymmetric conditions and small guide field. Our investigation indicates the observations correspond to an exhaust region 40 D_i downstream of the X line. The reconnection exhaust far away from the X line was typically regarded as a region where magnetohydrodynamic (MHD) processes dominate [*Vasyliunas*, 1975]. However, recent studies by *Le et al*. [2014] and *Fujimoto and Takamoto* [2016] have demonstrated the importance of the kinetic treatment in properly representing the exhaust of collisionless magnetic reconnection. Using particle-in-cell simulations, they found that kinetic process can lead to Hall effects (and signatures) that can extend up to 100 D_i downstream of the X line. Yet out-of-plane Hall magnetic field or possibly related electron signatures have been observed in reconnection exhausts, beyond the diffusion region, in the magnetotail and the solar wind [e.g., *Fujimoto et al*., 1997; *Nagai et al*., 2001; *Mistry et al*., 2017]. For the magnetopause, *Phan et al*. [2016a] recently showed evidence for electron-scale filamentary Hall currents in the exhaust and at its boundaries ~70 D_i downstream of the X line. Here we have reported on the full Hall magnetic field, electric field and current systems, which are found to maintain their large-scale structure (including their asymmetry) far from the X line in the exhaust of dayside magnetopause reconnection. The expected decoupling of ions and electrons, and associated Hall

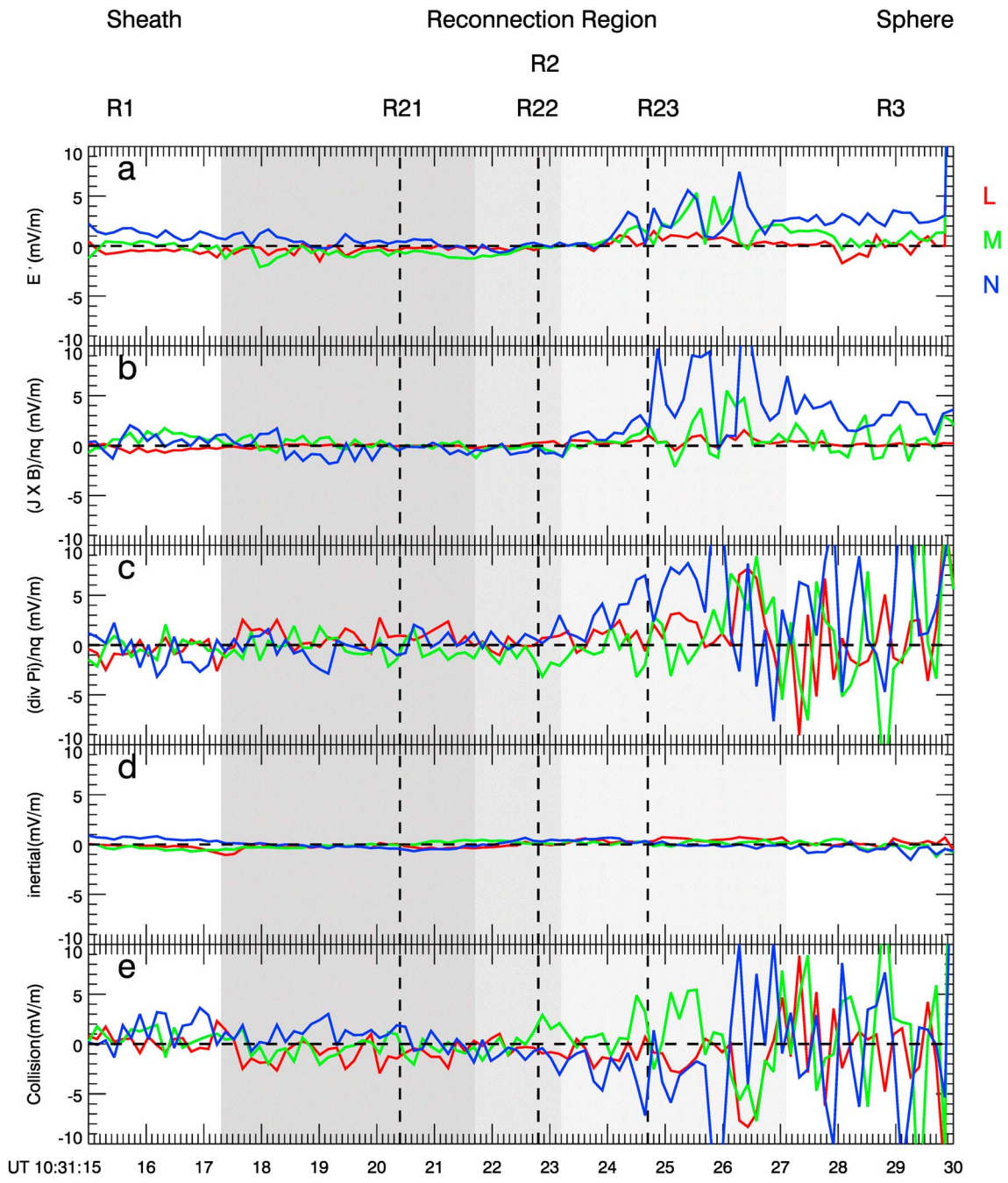

Figure 4. Results of the calculation of the terms of the electron and ion momentum equations. (a) the three components of the electric field $\boldsymbol{E}'=\boldsymbol{E}+\boldsymbol{V_i}\times\boldsymbol{B}$, (b) the three components of the Hall term $(\boldsymbol{J}\times\boldsymbol{B})/nq$ in the general Ohm's law, (c) the three components of the ion pressure gradient $(1/n_iq_i)\nabla\cdot\boldsymbol{P_i}$, (d) the three components of the ion inertial term $(m_i/q_i)\mathrm{d}\boldsymbol{V_i}/\mathrm{d}t$, and (e) the estimated three components of the collision term $(m_i/q_i)\nu_{\boldsymbol{ie}}(\boldsymbol{V_i}-\boldsymbol{V_e})$. The reconnection exhaust region is shaded grey.

current system, are clearly observed on both sides of the exhaust. These observations confirm that dynamic processes at particle scales extend far downstream the ion diffusion region. Apart from few studies, this possibility had been overlooked before the MMS era.

Thanks to MMS high-resolution particle measurements, the Hall current system is recovered from single-point measurements and the decoupling of ions and electrons can be analyzed in details. The complete in-plane current system was found to flow around the Hall magnetic fields, and the magnitude of the out-of-plane magnetic fields induced by this current is demonstrated to quantitatively agree with the

measured Hall magnetic field. This provides direct observational evidence for the process of Hall magnetic field generation by the Hall current system. We also found that the electron jet accelerated by parallel electric fields on the magnetospheric side strengthens the Hall currents, thereby compensating the otherwise lower density on the magnetospheric side (thought to be the source of the asymmetric Hall magnetic fields). In this event we further noted that the Hall current system is separated into two subsystems on the magnetosheath side. The reason for this separation is not clear. Multiple Hall currents, although at small scales, have been recently been reported in the exhaust region using MMS data [*Phan et al*., 2016a].

The normal electric fields associated with the Hall system are asymmetric in the present exhaust event, consistent with previous studies of the diffusion region. The 3-D electric field measurements and four-point plasma measurements make it possible to calculate each term in the ion momentum equation. Data suggest that the ion pressure gradient on the magnetospheric side is the main contributor to the normal electric field. The contribution from the inertial term is much lower. These findings provide observational additional evidences for the origin of the normal electric field associated with the Hall system, including in the exhaust region.

We now discuss the observed pattern of the Hall system. *Terasawa*, [1983] described Hall fields as a current layer eigenmode that consists of a tearing mode coupled with a shear Alfvén mode. The tearing mode itself does not have the out-of-plane B_y and the field-aligned currents. The out-of-plane Hall B_y (and V_y) and field-aligned currents are actually produced by the Alfvén wave perturbation. Recent theoretical studies have demonstrated the KAW nature of the Hall fields [*Dai*, 2009, *Shay et al*., 2011]. The pattern of Hall fields and currents can be explained by the polarization of the wave electric and magnetic fields and the current system of standing KAW. Standing KAW means that the KAW eigenmodes are standing along the normal direction of the current layer. In a reconnecting current layer, the current layer thickness is approximately the inhomogeneous scale along the normal direction, which is usually on the order of the ion inertial/gyroradius scale. The inhomogeneous scale is comparable to the perpendicular wavelength of the KAW. Under this condition the plane wave solution is not suitable and a KAW eigenmode description is needed. To a first approximation, we can replace k_x with $-i\partial_x$ in the dispersion relation of KAW plane wave [*Lee et al*., 1994; *Lysak and Lotko*, 1996; *Biskamp*, 2000], as *Dai* [2009] did. Then the obtained eigenmode differential equation yields a set of standing wave solution.

With regard to how KAW eigenmode can be excited, there are a number of possible scenarios. An imposed external reconnection electric field (E_M) can excite KAW eigenmode [*Dai*, 2009]. The KAW eigenmode may be excited by ion intrusion in the form of some profile of the ion current along the normal direction as well [*Dai et al*., 2016]. This is not a surprise. KAW eigenmode consists of many wave components (e.g., E_N, B_M, E_L, J_N, and J_L) which are coupled with E_M. Perturbations or a free energy source in any of these wave components may generate the KAW mode. Initially, as KAW eigenmode is excited, the KAW solution should be time dependent. The frequency ω of the KAW eigenmode is much less than the ion gyrofrequency. But ω is not zero in general. As the KAW eigenmode develops, the KAW solution may become steady state. $\omega = 0$ corresponds to the steady state solution.

An important prediction of KAW theory is that the ratio of Hall fields $|E_N|/|B_M|$ is on the order of 1 to a few Alfvén speeds based on the average profile of the current layer [*Dai*, 2009, *Shay et al*., 2011]. The observations show an average E_N of 5–10 mV/m and B_M of 10 nT on the magnetospheric side (Figures 1a and 1i). The ratio $|E_N|/|B_M|$ is in the range 500–1000 km/s. This value is a few times the Alfvén speed (250–800 km/s) on the magnetosphere side (Figure 1e), consistent with prediction of KAW theory. We note that similar $|E_N|/|B_M|$ ratios have been found in previous observations [e.g., *Mozer et al*., 2002; *Vaivads et al*., 2004; *Wygant et al*., 2005; *Duan et al*., 2016]. The same consistency also exists on the magnetosheath side, where the ratio $|E_N|/|B_M|$ is about 200 km/s and the Alfvén speed is in the range of 0–250 km/s. These consistent observations suggest that the Hall system can be explained by KAW theory in the exhaust region as well. Another important insight from KAW theory concerns the relation between the normal Hall electric field and the ion pressure gradient. Motivated by the present study and *Burch et al*. [2016], *Dai et al*. [2016] present the theoretical details of KAW physics which permits to support the normal electric field with the ion pressure gradient. Their theoretical deduction shows that the normal electric field results from magnetosheath ion intrusion through finite ion gyroradius effect in KAW.

In summary, the following conclusions are drawn from this work:

1. Asymmetric magnetic reconnection at the magnetopause can feature a full asymmetric Hall system downstream of the X line, all the way to 40 D_i in the exhaust region. The Hall system in the exhaust region inherits all features of the classic Hall system observed in the ion diffusion region. This implies that physics at particle scales plays a key role in the exhaust region, while MHD description was clearly prevailing before the MMS era.
2. The observed asymmetric Hall magnetic field directly results from the measured Hall currents, as demonstrated through the reconstruction of the out-of-plane Hall magnetic field component using a method based on Biot-Savart's law.
3. The asymmetric normal Hall electric field, on the other hand, appears to result from larger ion pressure gradients on the magnetospheric side of the exhaust, consistent with other recent studies.
4. The patterns of the Hall system are found to be consistent with KAW theory in the exhaust as well, i.e., as a manifestation of finite ion gyroradius effects in KAW. This fact witnesses the necessary stage of KAW propagation to further distance downstream along the current sheet [*Duan et al*., 2016] after its excitation in the reconnection diffusion region [*Dai*, 2009].

Acknowledgments
MMS data can be accessed at https://lasp.colorado.edu/mms/sdc/public/. We acknowledge all the MMS teams for their wonderful work. This work was supported by the National Natural Science Foundation of China (grants 41574163, 41574159, 41574161 and 41231066) and the Specialized Research Fund for State Key Laboratories. Work on MMS at IRAP is supported by CNRS and CNES.

References

Alexeev, I. V., C. J. Owen, A. N. Fazakerley, A. Runov, J. P. Dewhurst, A. Balogh, H. Réme, B. Klecker, and L. Kistler (2005), Cluster observations of currents in the plasma sheet during reconnection, *Geophys. Res. Lett.*, *32*, L03101, doi:10.1029/2004GL021420.

Andre, M., A. Vaivads, S. C. Buchert, A. N. Fazakerley, and A. Lahiff (2004), Thin electron-scale layers at the magnetopause, *Geophys. Res. Lett.*, *31*, L03803, doi:10.1029/2003GL018137.

Aunai, N., A. Retinò, G. Belmont, R. Smets, B. Lavraud, and A. Vaivads (2011), The proton pressure tensor as a new proxy of the proton decoupling region in collisionless magnetic reconnection, *Ann. Geophys.*, *29*, 1571–1579, doi:10.5194/angeo-29-1571-2011.

Biskamp, D. (2000), *Magnetic Reconnection in Plasmas*, pp. 29–80, Cambridge Univ. Press, Cambridge, U. K.

Borg, A. L., M. Øieroset, T. D. Phan, F. S. Mozer, A. Pedersen, C. Mouikis, J. P. McFadden, C. Twitty, A. Balogh, and H. Réme (2005), Cluster encounter of a magnetic reconnection diffusion region in the near Earth magnetotail on September 19, 2003, *Geophys. Res. Lett.*, *32*, L19105, doi:10.1029/2005GL023794.

Birn, J., et al. (2001), Geospace environmental modeling (GEM) magnetic reconnection challenge, *J. Geophys. Res.*, *106*, 3715–3720, doi:10.1029/1999JA900449.

Burch, J. L., T. E. Moore, R. B. Torbert, and B. L. Giles (2015), Magnetospheric Multiscale overview and science objectives, *Space Sci. Rev.*, 1–17, doi:10.1007/s11214-015-0164-9.

Burch, J. L., et al. (2016), Electron-scale measurements of magnetic reconnection in space, *Science*, doi:10.1126/science.aaf2939.

Cai, H. J., D. Q. Ding, and L. C. Lee (1994), Momentum transport near a magnetic X line in collisionless reconnection, *J. Geophys. Res.*, *99*(A1), 35–42, doi:10.1029/93JA02519.

Cai, H. J., and L. C. Lee (1997), The generalized Ohm's law in collisionless magnetic reconnection, *Phys. Plasmas*, *4*, 509–520, doi:10.1063/1.872178.

Cassak, P. A., and M. A. Shay (2007), Scaling of asymmetric magnetic reconnection: General theory and collisional simulations, *Phys. Plasmas*, *14*, 102114.

Cassak, P. A., and M. A. Shay (2008), Scaling of asymmetric Hall magnetic reconnection, *Geophys. Res. Lett.*, *35*, L19102, doi:10.1029/2008GL035268.

Cowley, S. W. H. (1995), Theoretical perspectives of the magnetopause: A tutorial review, in *Physics of the Magnetopause*, *Geophys. Monogr. Ser.*, vol. 90, edited by P. Song, B. U. O. Sonnerup, and M. F. Thomsen, pp. 29–44, AGU, Washington, D. C.

Dai, L. (2009), Collisionless magnetic reconnection via Alfvén eigenmodes, *Phys. Rev. Lett.*, *102*, 245003, doi:10.1103/PhysRevLett.102.245003.

Dai, L., C. Wang, V. Angelopoulos, and K.-H. Glassmeier (2015), In situ evidence of breaking the ion frozen-in condition via the non-gyrotropic pressure effect in magnetic reconnection, *Ann. Geophys.*, *33*, 1147–1153, doi:10.5194/angeo-33-1147-2015.

Dai, L., C. Wang, Y. Zhang, B. Lavraud, J. L. Burch, C. Pollock, and R. B. Torbert (2016), Kinetic Alfvén wave explanation of the Hall fields in magnetic reconnection, *Geophys. Res. Lett.*, *43*, 634–640, doi:10.1002/2016GL071044.

Deng, X. H., and H. Matsumoto (2001), Rapid magnetic reconnection in the Earth's magnetosphere mediated by whistler waves, *Nature*, *410*, 557–560.

Duan, S. P., L. Dai, C. Wang, J. Liang, A. T. Y. Lui, L. J. Chen, Z. H. He, Y. C. Zhang, and V. Angelopoulos (2016), Evidence of kinetic Alfvén eigenmode in the near-Earth magnetotail during substorm expansion phase, *J. Geophys. Res. Space Physics*, *121*, 4316–4330, doi:10.1002/2016JA022431.

Eastwood, J. P., M. A. Shay, T. D. Phan, and M. Øieroset (2010), Asymmetry of the diffusion region Hall electric and magnetic fields during guide field reconnection: Observations and comparison with simulations, *Phys. Rev. Lett.*, *104*, 205001.

Eastwood, J., T. D. Phan, M. Øieroset, M. A. Shay, K. Malakit, M. Swisdak, J. F. Drake, and A. Masters (2013), Influence of asymmetries and guide fields on the magnetic reconnection diffusion region in collisionless space plasmas, *Plasma Phys. Contr. F.*, *55*, 124001.

Eastwood, J. P., et al. (2016), Ion-scale secondary flux ropes generated by magnetopause reconnection as resolved by MMS, *Geophys. Res. Lett.*, *43*, 4716–4724, doi:10.1002/2016GL068747.

Egedal, J., M. Øieroset, W. Fox, and R. P. Lin (2005), In situ discovery of an electrostatic potential, trapping electrons and mediating fast reconnection in the Earth's magnetotail, *Phys. Rev. Lett.*, *94*, 025006.

Egedal, J., W. Fox, N. Katz, M. Porkolab, M. Øieroset, R. P. Lin, W. Daughton, and J. F. Drake (2008), Evidence and theory for trapped electrons in guide field magnetotail reconnection, *J. Geophys. Res.*, *113*, A12207, doi:10.1029/2008JA013520.

Fujimoto, K. (2014), Wave activities in separatrix regions of magnetic reconnection, *Geophys. Res. Lett.*, *41*, 2721–2728, doi:10.1002/2014GL059893.

Fujimoto, K., and M. Takamoto (2016), Ion and electron dynamics generating the Hall current in the exhaust far downstream of the reconnection x-line, *Phys. Plasmas*, *23*(1), doi:10.1063/1.4940322.
Fujimoto, M., M. S. Nakamura, I. Shinohara, T. Nagai, T. Mukai, Y. Saito, T. Yamamoto, and S. Kokubun (1997), Observations of earthward streaming electrons at the trailing boundary of a plasmoid, *Geophys. Res. Lett.*, *24*, 2893–2896, doi:10.1029/97GL02821.
Hesse, M., T. Neukirch, K. Schindler, M. Kuznetsova, and S. Zenitani (2011), The diffusion region in collisionless magnetic reconnection, *Space Sci. Rev.*, *160*, 3–23, doi:10.1007/s11214-010-9740-1.
Karimabadi, H., W. Daughton, and J. Scudder (2007), Multi-scale structure of the electron diffusion region, *Geophys. Res. Lett.*, *34*, L13104, doi:10.1029/2007GL030306.
Karimabadi, H., W. Daughton, and K. B. Quest (2005), Antiparallel versus component merging at the magnetopause: Current bifurcation and intermittent reconnection, *J. Geophys. Res.*, *110*, A03213, doi:10.1029/2004JA010750.
Khotyaintsev, Y. V., A. Vaivads, A. Retinò, M. André, C. J. Owen, and H. Nilsson (2006), Formation of inner structure of a reconnection separatrix region, *Phys. Rev. Lett.*, *97*, 20500.
Lavraud, B., et al. (2016), Currents and associated electron scattering and bouncing near the diffusion region at Earth's magnetopause, *Geophys. Res. Lett.*, *43*, 3042–3050, doi:10.1002/2016GL068359.
Le, A., J. Egedal, J. Ng, H. Karimabadi, J. Scudder, V. Roytershteyn, W. Daughton, and Y.-H. Liu (2014), Current sheets and pressure anisotropy in the reconnection exhaust, *Phys. Plasmas*, *21*, 012103.
Lee, L. C., J. R. Johnson, and Z. W. Ma (1994), Kinetic Alfvén waves as a source of plasma transport at the dayside magnetopause, *J. Geophys. Res.*, *99*(A9), 17,405–17,411, doi:10.1029/94JA01095.
Lysak, R. L., and W. Lotko (1996), On the kinetic dispersion relation for shear Alfvén waves, *J. Geophys. Res.*, *101*(A3), 5085–5094, doi:10.1029/95JA03712.
Malakit, K., M. A. Shay, P. A. Cassak, and C. Bard (2010), Scaling of asymmetric magnetic reconnection: Kinetic particle-in-cell simulations, *J. Geophys. Res.*, *115*, A10223, doi:10.1029/2010JA015452.
Manapat, M., M. Øieroset, T. D. Phan, R. P. Lin, and M. Fujimoto (2006), Field-aligned electrons at the lobe/plasma sheet boundary in the mid-to-distant magnetotail and their association with reconnection, *Geophys. Res. Lett.*, *33*, L05101, doi:10.1029/2005GL024971.
Mandt, M. E., R. E. Denton, and J. F. Drake (1994), Transition to whistler mediated magnetic reconnection, *Geophys. Res. Lett.*, *21*(1), 73–76, doi:10.1029/93GL03382.
Mistry, R., J. P. Eastwood, C. C. Haggerty, M. A. Shay, T. D. Phan, H. Hietala, and P. A. Cassak (2017), Observations of Hall reconnection physics far downstream of the X-line, *Phys. Rev. Lett.*, doi:10.1103/PhysRevLett.117.185102.
Mozer, F. S., S. D. Bale, and T. D. Phan (2002), Evidence of diffusion regions at a sub-solar magnetopause crossing, *Phys. Rev. Lett.*, *89*, 015002, doi:10.1103/PhysRevLett.89.015002.
Mozer, F. S., V. Angelopoulos, J. Bonnell, K. H. Glassmeier, and J. P. Mcfadden (2008a), THEMIS observations of modified Hall fields in asymmetric magnetic field reconnection, *Geophys. Res. Lett.*, *35*, L17S04, doi:10.1029/2007GL033033.
Mozer, F. S., P. L. Pritchett, J. Bonnell, D. Sundkvist, and M. T. Chang (2008b), Observations and simulations of asymmetric magnetic field reconnection, *J. Geophys. Res.*, *113*, A00C03, doi:10.1029/2008JA013535.
Nagai, T., I. Shinohara, M. Fujimoto, M. Hoshino, Y. Saito, S. Machida, and T. Mukai (2001), Geotail observations of the Hall current system: Evidence of magnetic reconnection in the magnetotail, *J. Geophys. Res.*, *106*, 25,929–25,949, doi:10.1029/2001JA900038.
Nagai, T., S. Zenitani, I. Shinohara, R. Nakamura, M. Fujimoto, Y. Saito, and T. Mukai (2013), Ion and electron dynamics in the ion-electron decoupling region of magnetic reconnection with Geotail observations, *J. Geophys. Res. Space. Physics*, *118*, 7703–7713, doi:10.1002/2013JA019135.
Øieroset, M., T. D. Phan, M. Fujimoto, R. P. Lin, and R. P. Lepping (2001), In situ detection of collisionless reconnection in the Earth's magnetotail, *Nature*, *412*, 414.
Øieroset, M., T. D. Phan, and M. Fujimoto (2004), Wind observations of asymmetric magnetic reconnection in the distant magnetotail, *Geophys. Res. Lett.*, *31*, L12801, doi:10.1029/2004GL019958.
Phan, T. D., and G. Paschmann (1996), Low-latitude dayside magnetopause and boundary layer for high magnetic shear: 1. Structure and motion, *J. Geophys. Res.*, *101*, 7801–7815, doi:10.1029/95JA03752.
Phan, T. D., et al. (2016a), MMS observations of electron-scale filamentary currents in the reconnection exhaust and near the X line, *Geophys. Res. Lett.*, *43*, 6060–6069, doi:10.1002/2016GL069212.
Phan, T. D., et al. (2016b), Ion Larmor radius effects near a reconnection X line at the magnetopause: THEMIS observations and simulation comparison, *Geophys. Res. Lett.*, *43*, 8844–8852, doi:10.1002/2016GL070224.
Pollock, C., et al. (2016), Fast plasma investigation for Magnetospheric Multiscale, *Space Sci. Rev.*, doi:10.1007/s11214-016-0245-4.
Pritchett, P. L. (2008), Collisionless magnetic reconnection in an asymmetric current sheet, *J. Geophys. Res.*, *113*, A06210, doi:10.1029/2007JA012930.
Paschmann, G., B. U. Ö. Sonnerup, I. Papamastorakis, N. Sckopke, G. Haerendel, S. J. Bame, J. R. Asbridge, J. T. Gosling, C. T. Russell, and R. C. Elphic (1979), Plasma acceleration at the Earth's magnetopause: Evidence for reconnection, *Nature*, *282*, 243–246, doi:10.1038/282243a0.
Russell, C. T., M. M. Mellott, E. J. Smith, and J. H. King (1983), Multiple spacecraft observations of interplanetary shocks: Four spacecraft determination of shock normals, *J. Geophys. Res.*, *88*, 4739–4748, doi:10.1029/JA088iA06p04739.
Russell, C. T., et al. (2015), The Magnetospheric Multiscale magnetometers, *Space Sci. Rev.*, doi:10.1007/s11214-014-0057-3.
Schwartz, S. J. (1998), Shock and discontinuity normals, Mach numbers and related parameters, in *Analysis Methods for Multi-Spacecraft Data*, edited by G. Paschmann and P. W. Daly, pp. 249–270, Int. Space Sci. Inst, Bern, Switzerland.
Shay, M. A., J. F. Drake, B. N. Rogers, and R. E. Denton (2001), Alfvénic collisionless magnetic reconnection and the Hall term, *J. Geophys. Res.*, *106*(A3), 3759–3772, doi:10.1029/1999JA001007.
Shay, M. A., J. F. Drake, J. P. Eastwood, and T. D. Phan (2011), Super-Alfvénic propagation of substorm reconnection signatures and Poynting flux, *Phys. Rev. Lett.*, *107*, 065001.
Sonnerup, B. U. Ö. (1979), Magnetic field reconnection, in *Solar System Plasma Physics*, edited by C. F. Kennel et al., pp. 45–108, Elsevier, North Holland, New York.
Sonnerup, B. U. Ö., and M. Scheible (1998), Minimum and maximum variation analysis, in *Analysis Methods for Multi-Spacecraft Data*, SR-001, edited by G. Paschmann and P. W. Daly, pp. 180–220, Int. Space Sci. Inst, Bern, Switzerland.
Sonnerup, B., G. Paschmann, S. Haaland, T. Phan, and S. Eriksson (2016), Reconnection layer bounded by switch-off shocks: Dayside magnetopause crossing by THEMIS D, *J. Geophys. Res. Space Physics*, *121*, 3310–3332, doi:10.1002/2016JA022362.
Swisdak, M., J. F. Drake, M. A. Shay, and J. G. McIlhargey (2005), Transition from antiparallel to component magnetic reconnection, *J. Geophys. Res.*, *110*, A05210, doi:10.1029/2004JA010748.
Terasawa, T. (1983), Hall current effect on tearing mode instability, *Geophys. Res. Lett.*, *10*, 475–478, doi:10.1029/GL010i006p00475.

Tharp, T. D., et al. (2012), Quantitative study of guide-field effects on Hall reconnection in a laboratory plasma, *Phys. Rev. Lett.*,109(16),165002.
Torbert, R. B., et al. (2014), The FIELDS instrument suite on MMS: Scientific objectives, measurements, and data products, *Space Sci. Rev.*, doi:10.1007/s11214-014-0109-8.
Torbert, R. B., et al. (2016), Estimates of terms in Ohm's law during an encounter with an electron diffusion region, *Geophys. Res. Lett.*, *43*, 5918–5925, doi:10.1002/2016GL069553.
Vasyliunas, V. M. (1975), Theoretical models of magnetic field line merging, *Rev. Geophys.*, *13*(1), 303–336, doi:10.1029/RG013i001p00303.
Vaivads, A., Y. Khotyaintsev, M. André, A. Retinò, S. C. Buchert, B. N. Rogers, P. Décréau, G. Paschmann, and T. D. Phan (2004), Structure of the magnetic reconnection diffusion region from four-spacecraft observations, *Phys. Rev. Lett.*, *93*, 105001.
Wang, S., et al. (2016), Two-scale ion meandering cause d by the polarization electric field during asymmetric reconnection, *Geophys. Res. Lett.*, *43*, 7831–7839, doi:10.1002/2016GL069842.
Wang, X., A. Bhattacharjee, and Z. W. Ma (2001), Scaling of collisionless forced reconnection, *Phys. Rev. Lett.*, *87*, 265003.
Wygant, J. R., et al. (2005), Cluster observations of an intense normal component of the electric field at a thin reconnecting current sheet in the tail and its role in the shock-like acceleration of the ion fluid into the separatrix region, *J. Geophys. Res.*, *110*, A09206, doi:10.1029/2004JA010708.
Xiao, C. J., et al. (2007), A Cluster measurement of fast magnetic reconnection in the magnetotail, *Geophys. Res. Lett.*, *34*, L01101, doi:10.1029/2006GL028006.
Zenitani, S., M. Hesse, A. Klimas, C. Black, and M. Kuznetsova (2011), The inner structure of collisionless magnetic reconnection: The electron-frame dissipation measure and Hall fields, *Phys. Plasmas*, *18*, 122108, doi:10.1063/1.3662430.